



**University of
Zurich**^{UZH}

**Zurich Open Repository and
Archive**

University of Zurich
University Library
Strickhofstrasse 39
CH-8057 Zurich
www.zora.uzh.ch

Year: 2017

Massive quenched galaxies at $z \approx 0.7$ retain large molecular gas reservoirs

Suess, Katherine A ; Bezanson, Rachel ; Spilker, Justin S ; Kriek, Mariska ; Greene, Jenny E ;
Feldmann, Robert ; Hunt, Qiana ; Narayanan, Desika

DOI: <https://doi.org/10.3847/2041-8213/aa85dc>

Posted at the Zurich Open Repository and Archive, University of Zurich

ZORA URL: <https://doi.org/10.5167/uzh-143826>

Journal Article

Published Version

Originally published at:

Suess, Katherine A; Bezanson, Rachel; Spilker, Justin S; Kriek, Mariska; Greene, Jenny E; Feldmann, Robert; Hunt, Qiana; Narayanan, Desika (2017). Massive quenched galaxies at $z \approx 0.7$ retain large molecular gas reservoirs. *Astrophysical Journal Letters*, 846(2):14.

DOI: <https://doi.org/10.3847/2041-8213/aa85dc>



Massive Quenched Galaxies at $z \sim 0.7$ Retain Large Molecular Gas Reservoirs

Katherine A. Suess¹ , Rachel Bezanson^{2,3} , Justin S. Spilker⁴ , Mariska Kriek¹ , Jenny E. Greene²,
Robert Feldmann⁵ , Qiana Hunt², and Desika Narayanan⁶

¹ Astronomy Department, University of California, Berkeley, CA 94720, USA; suess@berkeley.edu

² Department of Astrophysical Sciences, Princeton University, Princeton, NJ 08544, USA

³ Department of Physics and Astronomy and PITT PACC, University of Pittsburgh, Pittsburgh, PA 15260, USA

⁴ Steward Observatory, University of Arizona, 933 North Cherry Avenue, Tucson, AZ 85721, USA

⁵ Institute for Computational Science, University of Zurich, CH-8057 Zurich, Switzerland

⁶ Department of Astronomy, University of Florida, 211 Bryant Space Sciences Center, Gainesville, FL 32607, USA

Received 2017 July 13; revised 2017 August 7; accepted 2017 August 9; published 2017 September 1

Abstract

The physical mechanisms that quench star formation, turning blue star-forming galaxies into red quiescent galaxies, remain unclear. In this Letter, we investigate the role of gas supply in suppressing star formation by studying the molecular gas content of post-starburst galaxies. Leveraging the wide area of the Sloan Digital Sky Survey, we identify a sample of massive intermediate-redshift galaxies that have just ended their primary epoch of star formation. We present Atacama Large Millimeter/submillimeter Array CO(2-1) observations of two of these post-starburst galaxies at $z \sim 0.7$ with $M_* \sim 2 \times 10^{11} M_\odot$. Their molecular gas reservoirs of $(6.4 \pm 0.8) \times 10^9 M_\odot$ and $(34.0 \pm 1.6) \times 10^9 M_\odot$ are an order of magnitude larger than comparable-mass galaxies in the local universe. Our observations suggest that quenching does not require the total removal or depletion of molecular gas, as many quenching models suggest. However, further observations are required both to determine if these apparently quiescent objects host highly obscured star formation and to investigate the intrinsic variation in the molecular gas properties of post-starburst galaxies.

Key words: galaxies: evolution – galaxies: formation

1. Introduction

Galaxies at low and intermediate redshifts broadly fall into two categories: disk, blue star-forming galaxies and “quenched” red elliptical galaxies without ongoing star formation (e.g., Kauffmann et al. 2003). To create these observed galaxy populations, blue galaxies must somehow cease forming stars. Because stars form out of cold molecular gas, many quenching models attempt to explain the cessation of star formation through mechanisms that remove, deplete, or heat molecular gas reservoirs. For example, strong feedback from quasars could stop star formation by removing gas from the galaxy (e.g., Di Matteo et al. 2005; Hopkins et al. 2006), possibly induced by a major merger (e.g., Wellons et al. 2015). Massive molecular outflows, such as those observed locally by Alatalo (2015) and Leroy et al. (2015), could play a role in this process. Alternately, virial shocks could reduce the accretion of cool gas onto massive halos (e.g., Kereš et al. 2005; Dekel & Birnboim 2006) and prevent new stars from forming. Feldmann & Mayer (2015) suggest that star formation suppression is initiated by the decline of cool gas accretion onto the galaxy once the parent dark matter halo switches from a fast collapsing mode to a slow accretion mode.

To test these models, it is vital to investigate the molecular gas properties of galaxies just after they quench. Post-starburst galaxies—whose spectra resemble A-type stars, indicating a burst of star formation that ended ~ 1 Gyr ago (e.g., Le Borgne et al. 2006)—represent the direct and unpolluted products of the quenching process. Low-redshift post-starburst galaxies (“E+A” or “K+A” galaxies; e.g., Dressler & Gunn 1983; Couch & Sharples 1987; Zabludoff et al. 1996) have been shown to have larger molecular gas reservoirs than expected given their low star formation rates (SFRs; French et al. 2015). These low-mass galaxies are shutting off a small burst of late-time star formation,

as opposed to quenching their major star-forming episode. Only by moving to higher stellar masses and redshifts can we study galaxies that have just finished their primary epoch of star formation (e.g., Whitaker et al. 2012a); however, we must select galaxies at low enough redshifts that observations of low-J CO transitions are feasible.

In this Letter, we leverage the wide area of the Sloan Digital Sky Survey (SDSS; York et al. 2000) to identify post-starburst galaxies at $0.5 < z < 0.8$. We present Atacama Large Millimeter/submillimeter Array (ALMA) CO(2-1) observations of two $z \sim 0.7$ post-starburst galaxies, which reveal large reservoirs of molecular gas.

We assume a cosmology of $\Omega_m = 0.3$, $\Omega_\Lambda = 0.7$, and $h = 0.7$.

2. Sample Selection

To identify a sample of massive post-starburst galaxies bright enough for follow-up study, we select galaxies from the SDSS DR12 (Alam et al. 2015) spectroscopic catalog with $i < 19$, $z \geq 0.5$, and a median spectral signal-to-noise ratio > 3.7 . We identify galaxies dominated by A-type stars following the method introduced in Kriek et al. (2010), which selects post-starburst galaxies by their strong Balmer breaks and their blue slopes redward of the break. The final selection was checked by eye to remove stars and brown dwarfs, and consists of 50 post-starburst galaxies at $0.5 \leq z \leq 0.8$ with a median redshift of $z = 0.6$.

To derive the stellar masses of the post-starburst galaxy sample, we fit the SDSS spectra with the stellar population synthesis fitting code FAST (Kriek et al. 2009) using the Bruzual & Charlot (2003) stellar population library, a Chabrier (2003) initial mass function (IMF), a delayed exponential star formation history, and the Kriek & Conroy (2013) dust attenuation law. The mass was aperture corrected using the difference between the photometric magnitude in the SDSS g ,

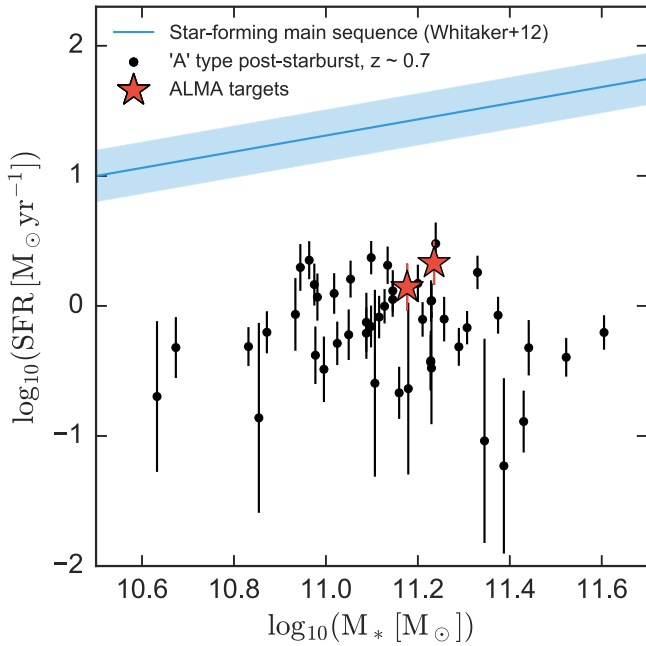


Figure 1. SFR, estimated using the dust-corrected [O II] $\lambda 3727$ luminosity, as a function of stellar mass for “A-type” post-starburst galaxies selected from the SDSS. Red stars indicate the galaxies observed with ALMA. The blue shaded line indicates the star-forming main sequence at $z = 0.6$ from Whitaker et al. (2012b); all post-starburst galaxies in the sample lie significantly below the main sequence.

r , and i filters and the same magnitudes as measured from the optical spectra; this correction increased the adopted stellar mass by a mean factor of 1.5.

We measured SFRs using the aperture-corrected line flux of the [O II] $\lambda 3727$ doublet and the SFR conversion in Kennicutt (1998a), adjusted to a Chabrier IMF. To measure the [O II] flux, we modeled the region around the doublet as a single Gaussian centered at the mean wavelength of [O II] plus a straight-line continuum with a free slope and intercept. The width of the Gaussian line was held equal to the stellar velocity dispersion, given in the MPA-JHU catalogs (Aihara et al. 2011). In all cases, the velocity dispersion resulted in a single Gaussian wider than the separation between the two lines in the [O II] doublet. Uncertainties in the SFR were bootstrapped from 1000 realizations of the [O II] line flux fit. We corrected the SFR for dust attenuation using the best-fit dust attenuation value from the stellar population fit (median $A_v = 0.8$ mag).

Figure 1 shows the SFR as a function of stellar mass for the full post-starburst galaxy sample. All galaxies lie significantly below the star-forming main sequence at this redshift (Whitaker et al. 2012b).

3. ALMA Observations

We selected two of the highest-redshift, brightest galaxies—SDSS J0912+1523 and SDSS J2202-0033—from the full sample for follow-up observations with ALMA. The SDSS discovery spectra of these two galaxies are shown in Figure 2, and basic parameters are listed in Table 1. The ALMA observations were carried out in program 2016.1.01126.S (PI: R. Bezanson) in 2017 January and March using the ALMA Band 4 receivers (Asayama et al. 2014). Observations were made in 80 minute blocks, with two blocks dedicated to each target. The total on-source integration time for each target was ~ 100 minutes. The data were reduced using the standard

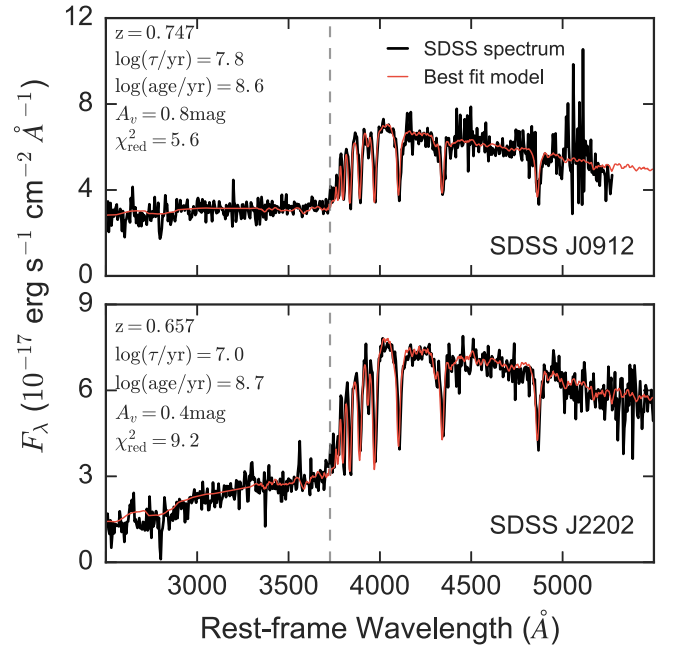


Figure 2. SDSS discovery spectra of SDSS J0912+1523 and SDSS J2202-0033. Best-fit stellar population synthesis models are overlaid in red. The gray dashed line indicates the location of the [O II] $\lambda 3727$ doublet used to measure the SFR.

ALMA pipeline, which produced good results for both SDSS J0912+1523 observing blocks and one SDSS J2202-0033 block. In the second observation of SDSS J2202-0033, many antennas were shadowed by other antennas during observations of the bandpass calibrator due to the compact array configuration. This caused the automatic pipeline to flag the shadowed antennas for the remainder of the observing block. We instead derived the frequency-dependent response of the affected antennas using the repeated observations of the complex gain calibrator carried out during the remainder of the track. While the gain calibrator is not as bright as the bandpass calibrator, we verified that the bandpass solutions derived in this way are consistent with those using the bandpass calibrator for the antennas that were not shadowed.

The observations reach a spatial resolution of $2''.2 \times 3''.0$ (16×22 kpc) and $1''.7 \times 2''.4$ (12×17 kpc) for SDSS J2202-0033 and SDSS J0912+1523, respectively, in images inverted using natural weighting, which maximizes sensitivity at the expense of slightly lower spatial resolution. No 2 mm continuum emission was detected in either source, with a 3σ upper limit $< 75 \mu\text{Jy}$.

CO(2–1) is significantly detected in both target galaxies. Inspection of the image cubes and a comparison of the maximum pixel values with the integrated flux density indicate that SDSS J0912+1523 is marginally spatially resolved, with a deconvolved source FWHM of $1''.9 \pm 0''.3$ (14 ± 2 kpc). SDSS J2202-0033 is not spatially resolved at the depth and resolution of our data. To extract spectra, we fit a point source (SDSS J2202-0033) or a circular Gaussian (SDSS J0912+1523) to the visibility data using the *uvmultifit* package (Martí-Vidal et al. 2014), averaging 24 (SDSS J2202-0033) or 6 (SDSS J0912+1523) channels, yielding a velocity resolution of ~ 200 and 50 km s^{-1} , respectively. These spectra, as well as images integrated over the full line widths of each target, are shown in Figure 3.

Table 1
Post-starburst Targets

ID	z	M_* (M_\odot)	SFR ($M_\odot \text{ yr}^{-1}$)	Aperture Correction	L_{CO} ($\text{K km s}^{-1} \text{ pc}^2$)	M_{gas} (M_\odot)
SDSS J0912+1523	0.747	$(1.7 \pm 0.3) \times 10^{11}$	2.1 ± 0.8	1.13 ± 0.01	8.5 ± 0.4	$(34.0 \pm 1.6) \times 10^9$
SDSS J2202-0033	0.657	$(1.5 \pm 0.2) \times 10^{11}$	1.4 ± 0.6	1.11 ± 0.01	1.6 ± 0.2	$(6.4 \pm 0.8) \times 10^9$

Note. Errors in M_* are dominated by systematics, which we estimated by varying the model library, star formation history, and dust law in the stellar population fits.

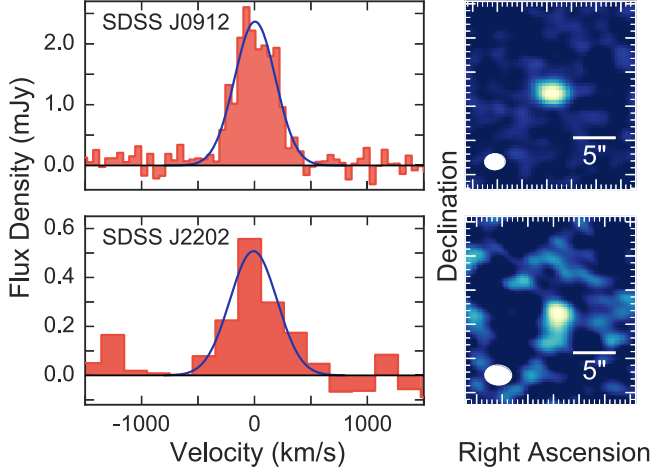


Figure 3. Left: ALMA CO(2–1) spectra for each target. The blue line shows the best-fit Gaussian used to extract the total line flux. Right: integrated line images for each target. The white oval shows the ALMA beam.

4. Molecular Gas Masses

Both sources are significantly detected in CO(2–1) emission (see Figure 3). We fit simple Gaussian profiles to these spectra, which yield integrated line fluxes of 1.07 ± 0.05 and $0.27 \pm 0.03 \text{ Jy km s}^{-1}$ for SDSS J0912+1523 and SDSS J2202-0033, respectively. At the redshifts of each source, these fluxes correspond to line luminosities $L'_{\text{CO}} = 8.5 \pm 0.4$ and $1.6 \pm 0.2 \times 10^9 \text{ K km s}^{-1} \text{ pc}^2$, respectively.

The CO line luminosity can be converted to a molecular gas mass using the conversion factor α_{CO} . In high-metallicity objects, α_{CO} typically varies from $\approx 0.8 M_\odot / (\text{K km s}^{-1} \text{ pc}^2)$ in highly star-forming objects (typically gas-rich merging systems) to $\approx 4 M_\odot / (\text{K km s}^{-1} \text{ pc}^2)$ in the Milky Way and other normal star-forming galaxies, principally due to the escape probability in the optically thick CO line (see Bolatto et al. 2013 for a recent review; hereafter we suppress the units of α_{CO}).

We estimate the value of α_{CO} using the numerical models of Narayanan et al. (2012). These authors combined hydrodynamical modeling of a variety of isolated and merging galaxies with molecular line radiative transfer to develop a fitting formula for α_{CO} as a function of the CO surface brightness. SDSS J2202-0033 is not spatially resolved at the depth and resolution of our data, which yields a lower limit on the CO surface brightness and an upper limit on the conversion factor of $\alpha_{\text{CO}} \lesssim 7.0$. Our data spatially resolve SDSS J0912+1523; combined with its CO luminosity, this implies $\alpha_{\text{CO}} \sim 3.5$. For ease of comparison with the literature, we therefore adopt $\alpha_{\text{CO}} = 4.0$ for both of our targets.

Additionally, α_{CO} is valid and applies only to the CO(1–0) transition, so observations of higher CO lines require a correction factor to the ground state. Based on observations

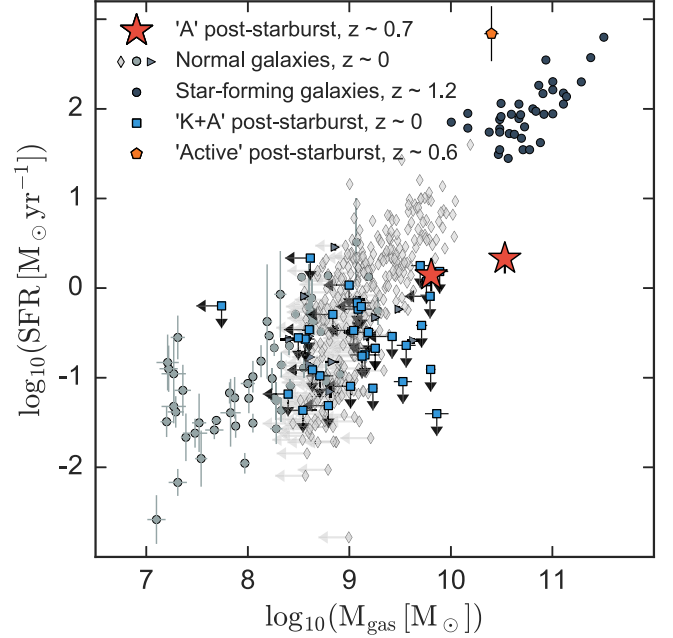


Figure 4. SFR as a function of molecular gas mass for SDSS J2202-0033 and SDSS J0912+1523 (red stars) as well as comparison samples. Blue squares indicate the French et al. (2015) low-redshift “K+A” post-starburst galaxies; all SFRs are upper limits due to possible LINER emission. Dark gray points are star-forming galaxies from PHIBSS at $z \sim 1.2$. Gray diamonds are normal galaxies from COLDGASS, gray circles are from ATLAS-3D, and gray triangles are from MASSIVE. The orange pentagon is an “active” post-starburst galaxy identified in Sell et al. (2014), with a gas mass measured by Geach et al. (2013). All have been normalized to $\alpha_{\text{CO}} = 4$. SDSS J0912+1523 and SDSS J2202-0033 are clearly offset from star-forming galaxies at both $z \sim 0$ and $z \sim 1.2$.

of a wide variety of galaxies at many redshifts, the CO(2–1)/CO(1–0) line ratio likely falls in the range 0.7–1.0 in temperature units, where 1.0 indicates thermalized emission (e.g., Combes et al. 2007; Dannerbauer et al. 2009; Young et al. 2011). We assume thermalized emission in our analysis. This is a conservative assumption, yielding a minimum CO(1–0) line luminosity; the true values may be higher by $\approx 30\%$.

Given these assumptions, we find molecular gas masses of $M_{\text{gas}} = (34.0 \pm 1.6) \times 10^9 M_\odot$ for SDSS J0912+1523 and $M_{\text{gas}} = (6.4 \pm 0.8) \times 10^9 M_\odot$ for SDSS J2202-0033. These uncertainties reflect only the statistical uncertainties on the measured CO luminosities; we stress that there are also factor of two systematic uncertainties associated with the CO excitation and conversion factor.

In Figure 4, we show SFR versus molecular gas mass for SDSS J0912+1523 and SDSS J2202-0033. It is clear that our observations, especially SDSS J0912+1523, are significantly offset from measurements of star-forming galaxies at both low and high redshifts. Adopting the CO size, the gas mass surface density of SDSS J0912+1523 is a factor of 11 higher than

expected from its SFR surface density (Kennicutt 1998b). SDSS J0912+1523 has a gas mass a factor of two larger than expectations from the empirical scaling relation in Genzel et al. (2015); SDSS J2202-0033 has a gas mass three times lower than expected from the same scaling.

In Figure 4, we show for comparison the low-redshift “K+A” post-starburst galaxies in French et al. (2015), an “active” post-starburst galaxy in the Sell et al. (2014) sample observed in CO by Geach et al. (2013), and star-forming and quiescent galaxies at $z \sim 0$ (COLDGASS, Saintonge et al. 2011; ATLAS-3D, Cappellari et al. 2011, 2013; Young et al. 2011; Davis et al. 2013, 2014; and MASSIVE, Davis et al. 2016) as well as $z \sim 1.2$ (PHIBSS; Tacconi et al. 2013). Molecular gas fractions ($f_{\text{gas}} \equiv M_{\text{gas}}/M_*$) vary significantly both among the three post-starburst samples and within in each sample: the K+A post-starbursts have $f_{\text{gas}} \sim 1\%$ –40%, the active post-starburst has $f_{\text{gas}} \sim 19\%$, and SDSS J0912+1523 and SDSS J2202-0033 have $f_{\text{gas}} \sim 20\%$ and 4%, respectively.

5. Implications for Galaxy Quenching

Our results imply that star formation can be suppressed in galaxies that still have significant reservoirs of molecular gas. Models that require the complete depletion or ejection of molecular gas to quench star formation are inconsistent with the large gas masses in SDSS J0912+1523 and SDSS J2202-0033. Models that explain star formation suppression without removing the gas—such as morphological quenching (Martig et al. 2009), which suggests that a buildup of stars into a bulge can stabilize some cold molecular gas against collapse—are more consistent with our observations. However, it is not clear that current quenching models can fully explain the observed elevated molecular gas masses, especially for SDSS J0912+1523.

Alternatively, the star formation in SDSS J0912+1523 and SDSS J2202-0033 may only be temporarily suppressed. Simulations of massive $z \sim 2$ galaxies predict a large amount of variability in interstellar medium properties and star formation activity on short (\sim tens of Myr) timescales (Feldmann et al. 2017). These simulations contain a small number of galaxies with molecular gas fractions and SFR/M_* similar to SDSS J2202-0033. However, they are not able to reproduce a counterpart of the more extreme case of SDSS J0912+1523.

The factor of five difference in gas mass between SDSS J0912+1523 and SDSS J2202-0033 indicates that, unsurprisingly, quenching may proceed differently from galaxy to galaxy. A larger galaxy sample is required to investigate intrinsic variations in the gas properties of post-starburst galaxies and determine whether SDSS J0912+1523 is an intriguing outlier or is representative of recently quenched galaxies.

6. Comparison to Other Studies

Our results are similar to French et al. (2015), who found high molecular gas masses given the SFR of “K+A” post-starburst galaxies at $0.01 < z < 0.12$. These authors interpret their observations as evidence for suppressed star formation efficiency, a low α_{CO} , or a bottom-heavy IMF in these galaxies.

There are, however, significant differences between the French et al. (2015, hereafter “K+A sample”) post-starburst galaxies, the post-starburst galaxies in this study, and the post-starburst galaxies in other studies such as Sell et al. (2014, hereafter “active sample”). The K+A sample includes

$z < 0.12$, $M_* \sim 10^{10.6} M_\odot$ galaxies with strong Balmer lines and low ongoing star formation. The active sample includes $z \sim 0.6$, $M_* = 10^{10.5} - 10^{11.5} M_\odot$ galaxies with strong Balmer absorption and weak nebular emission. In this study, we select $z \sim 0.6$, $M_* \sim 10^{11.1} M_\odot$ galaxies with strong Balmer breaks and blue slopes redward of the break. Despite all selections emphasizing “post-burst” criteria, the median stacked optical spectra of the three samples (top panel of Figure 5) are clearly distinct. The active sample shows prominent UV continuum as well as [O II] and [O III] emission lines; inferred SFRs are $\sim 300 M_\odot \text{ yr}^{-1}$. The K+A sample does not show UV continuum or emission lines, but has excess emission at rest-frame $\lambda \gtrsim 4500 \text{ \AA}$ indicating a larger fractional contribution from old stars than the “A-type” post-starburst selection in this Letter.

To further illustrate the differences between the post-starburst samples, we show the $H\delta_A$ index as a function of D_n4000 for all three samples as well as SDSS DR12 galaxies with $0.05 \leq z \leq 0.07$ and $M_\odot \geq 10^{10} M_\odot$ (bottom panel of Figure 5). The $H\delta_A$ index traces recent star formation, and D_n4000 is sensitive to the age of the stellar population. For all three post-starburst samples we measured $H\delta_A$ using EZ_Ages (Graves & Schiavon 2008), adopting the Princeton 1D VDISP measurement for the velocity dispersion correction; we measured D_n4000 from the SDSS spectra (Balogh et al. 1999). Purple lines of increasing shade indicate the time evolution of Bruzual & Charlot (2003) single-/double-burst models with an increasing contribution from old stars. The first model is a simple stellar population; the second is a model where 90% of the stars were formed in a starburst 4 Gyr before the current star formation epoch; the third is a model where 95% of the stars were formed in a previous starburst.

The active sample lies at low D_n4000 and has a range of $H\delta_A$ values likely corresponding to emission partially filling in the $H\delta$ absorption feature. Given their high inferred SFR, these galaxies are still “active” and have not yet fully quenched their star formation; it is possible that after they quench, these galaxies will resemble A-type post-starburst galaxies. The K+A post-starbursts are consistent with models where only 5%–10% of the galaxy’s mass was formed in the most recent burst. This indicates that these galaxies formed the majority of their stars at higher redshift and have just quenched a small amount of late-time star formation. Their spectra show the signatures of recently formed A-type stars as well as older K-type stars from previous star formation episodes. The A-type post-starbursts selected in this Letter are consistent with a simple stellar population model, i.e., they likely just finished their primary epoch of star formation and thus look like A-type stars.

Given these differences, it is not clear that the same physical mechanisms should quench both the late-time star formation in the $z \sim 0$ K+A galaxies and the primary epoch of star formation in the $z \sim 0.7$ A-type post-starburst galaxies. It is surprising that both the low-redshift K+A post-starbursts and intermediate-redshift A-type post-starbursts show high gas molecular gas masses for their SFR, indicating quenching in both redshift regimes can occur without exhausting or depleting molecular gas reservoirs.

7. Discussion

In this Letter, we present ALMA CO(2-1) observations of two recently quenched post-starburst galaxies at $z \sim 0.7$. These galaxies were selected from a unique sample of 50

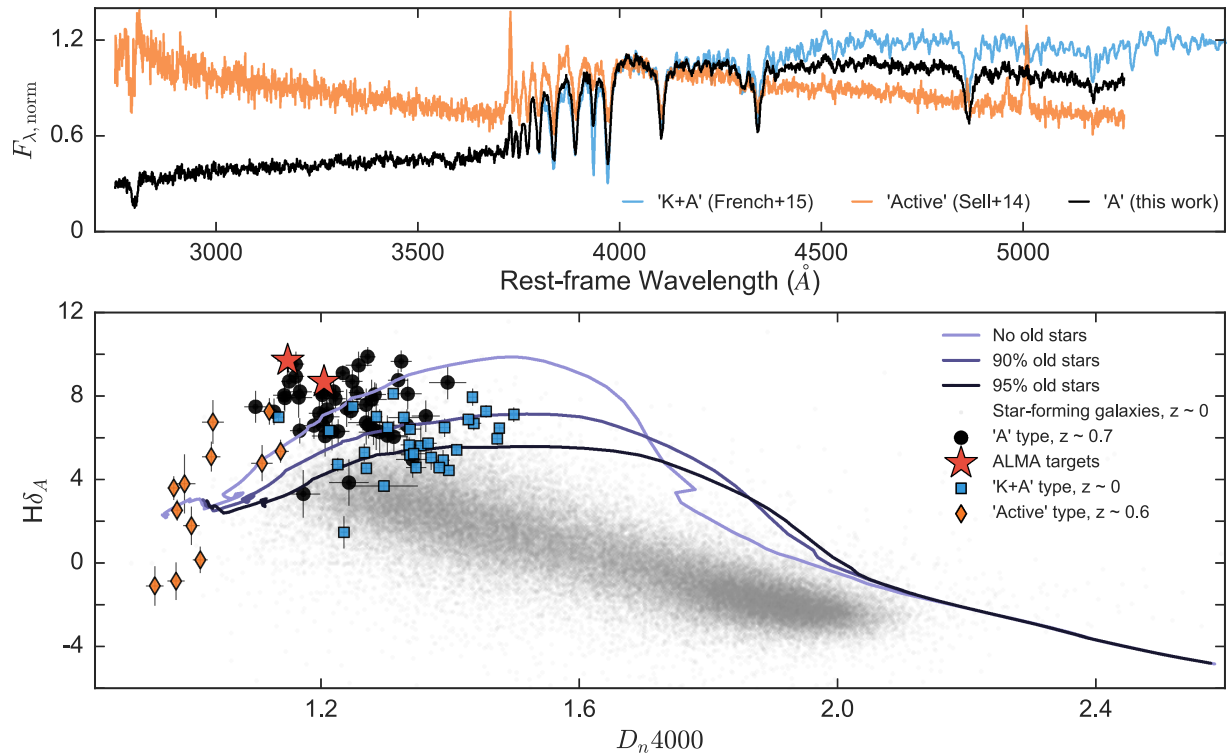


Figure 5. Top: median stacked spectra of “K+A” (French et al. 2015; blue), “active” (Sell et al. 2014; orange), and “A” type (black) post-starburst galaxies. Bottom: $H\delta_A$ vs. D_n4000 for the same three post-starburst samples. ALMA targets are shown with red stars; SDSS galaxies are shown in gray. Purple lines indicate Bruzual & Charlot (2003) models where 0%, 90%, and 95% of stars were formed in a previous burst. As time increases, the model tracks evolve left to right.

A-type post-starburst galaxies at $z \sim 0.6$. Unlike low-redshift K+A post-starburst galaxies, these massive galaxies have just concluded their major star-forming episode. Additionally, this sample lies at low enough redshift that follow-up observations of low-J CO transitions are feasible. The observed molecular gas masses in these galaxies are significantly higher than expected given their low ongoing SFR. This indicates that galaxies may quench their primary epoch of star formation without completely depleting or exhausting their molecular gas.

However, there are several alternative explanations for the high gas masses in SDSS J0912+1523 and SDSS J2202-0033. Short-term SFR variations, seen in some higher-redshift galaxy simulations, could account for the elevated gas mass of SDSS J2202-0033. As in French et al. (2015), a lower α_{CO} value could decrease the inferred gas mass and a bottom-heavy IMF could increase the inferred SFR, alleviating tension between the gas supply and low ongoing SFR. It is also possible that there is significant obscured star formation in SDSS J0912+1523 or SDSS J2202-0033.

We place a constraint on the dust-obscured star formation of each target using the non-detection of the 2 mm ALMA continuum. We assume that the dust emission follows a standard modified blackbody function with $T_{\text{dust}} = 30$ K (typical of star-forming galaxies; e.g., Magdis et al. 2012). The resulting upper limits on the FIR luminosity imply 3σ upper limits on the obscured SFR $\lesssim 50 M_{\odot} \text{ yr}^{-1}$. We additionally constrain the obscured star formation with *Wide-field Infrared Survey Explorer* (WISE) 12 μm data (Mainzer et al. 2011), using the log average of Dale & Helou (2002) templates with $1 \leq \alpha \leq 2.5$ to convert the observed 12 μm luminosity to a total IR luminosity, following Whitaker et al. (2012b); this gives an upper limit of $\sim 60 M_{\odot} \text{ yr}^{-1}$. Just $\sim 6 M_{\odot} \text{ yr}^{-1}$ of obscured star formation—well below the current constraints from either WISE

or 2 mm continuum—would place SDSS J2202-0033 in line with the expected relation. In contrast, $\sim 60 M_{\odot} \text{ yr}^{-1}$ of obscured star formation is required to account for the significant gas reservoir in SDSS J0912+1523. Both the radio and infrared SFR upper limits are highly uncertain, and deeper rest-frame infrared measurements are required to place stronger constraints on any obscured star formation.

Finally, we note that the sample size of this study is very small; measurements of the molecular gas in a larger sample of post-starburst galaxies are necessary to determine if these galaxies are simply outliers. Thus, moving forward we need to obtain a larger sample of galaxies with gas measurements and tight constraints on the dust-obscured SFR. By studying the intrinsic variation in molecular gas properties of A-type post-starburst galaxies, we may be able to constrain the primary mechanisms behind galaxy quenching.

This paper makes use of the following ALMA data: ADS/JAO.ALMA #2016.1.00126.S. ALMA is a partnership of ESO (representing its member states), NSF (USA) and NINS (Japan), together with NRC (Canada), NSC and ASIAA (Taiwan), and KASI (Republic of Korea), in cooperation with the Republic of Chile. The Joint ALMA Observatory is operated by ESO, AUI/NRAO and NAOJ. This material is based upon work supported by the National Science Foundation Graduate Research Fellowship Program under grant No. DGE 1106400. K.A.S. also acknowledges support from the University of California, Berkeley Chancellor’s Fellowship. J.E.G. is supported in part by NSF AST-1411642. R.F. acknowledges financial support from the Swiss National Science Foundation (grant 157591). D.N. was supported by NSF AST-1724864 and HST AR-13906.001.

ORCID iDs

Katherine A. Suess  <https://orcid.org/0000-0002-1714-1905>
 Rachel Bezanson  <https://orcid.org/0000-0001-5063-8254>
 Justin S. Spilker  <https://orcid.org/0000-0003-3256-5615>
 Mariska Kriek  <https://orcid.org/0000-0002-7613-9872>
 Robert Feldmann  <https://orcid.org/0000-0002-1109-1919>
 Desika Narayanan  <https://orcid.org/0000-0002-7064-4309>

References

- Aihara, H., Allende Prieto, C., An, D., et al. 2011, *ApJS*, **193**, 29
 Alam, S., Albareti, F. D., Allende Prieto, C., et al. 2015, *ApJS*, **219**, 12
 Alatalo, K. 2015, *ApJL*, **801**, L17
 Asayama, S., Takahashi, T., Kubo, K., et al. 2014, *PASJ*, **66**, 57
 Balogh, M. L., Morris, S. L., Yee, H. K. C., Carlberg, R. G., & Ellingson, E. 1999, *ApJ*, **527**, 54
 Bolatto, A. D., Wolfire, M., & Leroy, A. K. 2013, *ARA&A*, **51**, 207
 Bruzual, G., & Charlot, S. 2003, *MNRAS*, **344**, 1000
 Cappellari, M., Emsellem, E., Krajnović, D., et al. 2011, *MNRAS*, **413**, 813
 Cappellari, M., Scott, N., Alatalo, K., et al. 2013, *MNRAS*, **432**, 1709
 Chabrier, G. 2003, *PASP*, **115**, 763
 Combes, F., Young, L. M., & Bureau, M. 2007, *MNRAS*, **377**, 1795
 Couch, W. J., & Sharples, R. M. 1987, *MNRAS*, **229**, 423
 Dale, D. A., & Helou, G. 2002, *ApJ*, **576**, 159
 Dannerbauer, H., Daddi, E., Riechers, D. A., et al. 2009, *ApJL*, **698**, L178
 Davis, T. A., Alatalo, K., Bureau, M., et al. 2013, *MNRAS*, **429**, 534
 Davis, T. A., Greene, J., Ma, C.-P., et al. 2016, *MNRAS*, **455**, 214
 Davis, T. A., Young, L. M., Crocker, A. F., et al. 2014, *MNRAS*, **444**, 3427
 Dekel, A., & Birnboim, Y. 2006, *MNRAS*, **368**, 2
 Di Matteo, T., Springel, V., & Hernquist, L. 2005, *Natur*, **433**, 604
 Dressler, A., & Gunn, J. E. 1983, *ApJ*, **270**, 7
 Feldmann, R., & Mayer, L. 2015, *MNRAS*, **446**, 1939
 Feldmann, R., Quataert, E., Hopkins, P. F., Faucher-Giguère, C.-A., & Kereš, D. 2017, *MNRAS*, **470**, 1050
 French, K. D., Yang, Y., Zabludoff, A., et al. 2015, *ApJ*, **801**, 1
 Geach, J. E., Hickox, R. C., Diamond-Stanic, A. M., et al. 2013, *ApJL*, **767**, L17
 Genzel, R., Tacconi, L. J., Lutz, D., et al. 2015, *ApJ*, **800**, 20
 Graves, G. J., & Schiavon, R. P. 2008, *ApJS*, **177**, 446
 Hopkins, P. F., Hernquist, L., Cox, T. J., et al. 2006, *ApJS*, **163**, 1
 Kauffmann, G., Heckman, T. M., White, S. D. M., et al. 2003, *MNRAS*, **341**, 54
 Kennicutt, R. C., Jr. 1998a, *ARA&A*, **36**, 189
 Kennicutt, R. C., Jr. 1998b, *ApJ*, **498**, 541
 Kereš, D., Katz, N., Weinberg, D. H., & Davé, R. 2005, *MNRAS*, **363**, 2
 Kriek, M., & Conroy, C. 2013, *ApJL*, **775**, L16
 Kriek, M., Labbé, I., Conroy, C., et al. 2010, *ApJL*, **722**, L64
 Kriek, M., van Dokkum, P. G., Labbé, I., et al. 2009, *ApJ*, **700**, 221
 Le Borgne, D., Abraham, R., Daniel, K., et al. 2006, *ApJ*, **642**, 48
 Leroy, A. K., Walter, F., Martini, P., et al. 2015, *ApJ*, **814**, 83
 Magdis, G. E., Daddi, E., Béthermin, M., et al. 2012, *ApJ*, **760**, 6
 Mainzer, A., Bauer, J., Grav, T., et al. 2011, *ApJ*, **731**, 53
 Martig, M., Bournaud, F., Teyssier, R., & Dekel, A. 2009, *ApJ*, **707**, 250
 Martí-Vidal, I., Vlemmings, W. H. T., Muller, S., & Casey, S. 2014, *A&A*, **563**, A136
 Narayanan, D., Krumholz, M. R., Ostriker, E. C., & Hernquist, L. 2012, *MNRAS*, **421**, 3127
 Saintonge, A., Kauffmann, G., Kramer, C., et al. 2011, *MNRAS*, **415**, 32
 Sell, P. H., Tremonti, C. A., Hickox, R. C., et al. 2014, *MNRAS*, **441**, 3417
 Tacconi, L. J., Neri, R., Genzel, R., et al. 2013, *ApJ*, **768**, 74
 Wellons, S., Torrey, P., Ma, C.-P., et al. 2015, *MNRAS*, **449**, 361
 Whitaker, K. E., Kriek, M., van Dokkum, P. G., et al. 2012a, *ApJ*, **745**, 179
 Whitaker, K. E., van Dokkum, P. G., Brammer, G., & Franx, M. 2012b, *ApJL*, **754**, L29
 York, D. G., Adelman, J., Anderson, J. E., Jr., et al. 2000, *AJ*, **120**, 1579
 Young, L. M., Bureau, M., Davis, T. A., et al. 2011, *MNRAS*, **414**, 940
 Zabludoff, A. I., Zaritsky, D., Lin, H., et al. 1996, *ApJ*, **466**, 104